Polarization-locked vector solitons in a mode-locked fiber laser using polarization-sensitive few-layer graphene deposited D-shaped fiber saturable absorber

Tao Chen,[1,2,3] Changrui Liao,[2,4] D. N. Wang,[1,2,5,*] and Yiping Wang[4]

[1]*College of Optical and Electronic Technology, China Jiliang University, Hangzhou, China*
[2]*Department of Electrical Engineering, The Hong Kong Polytechnic University, Hong Kong, China*
[3]*School of Physics and Technology, University of Jinan, Jinan, Shandong 250022, China*
[4]*College of Optoelectronic Engineering, Shenzhen University, Shenzhen, Guangdong 518060, China*
[5]*School of Electrical, Electronic and Information Engineering, Hubei Polytechnic University, Huangshi, China*
**Corresponding author: eednwang@polyu.edu.hk*

Received December 19, 2013; revised March 21, 2014; accepted April 13, 2014;
posted April 25, 2014 (Doc. ID 203351); published May 27, 2014

We have experimentally demonstrated polarization-locked vector soliton generation in a passively mode-locked erbium-doped fiber laser by using a few-layer graphene deposited D-shaped fiber to act as a saturable absorber (SA). Due to the long light/graphene interaction length and the asymmetric structure, the SA used in this work has large polarization-dependent loss, and as a result, the stationary polarization-locked vector solitons can be generated, being different from the scalar solitons produced by the nonlinear polarization rotation technique. The formation mechanism of such solitons is studied and it is found that they are elliptically polarized solitons. © 2014 Optical Society of America

OCIS codes: (140.3510) Lasers, fiber; (140.4050) Mode-locked lasers; (140.7090) Ultrafast lasers; (320.5550) Pulses.

http://dx.doi.org/10.1364/JOSAB.31.001377

1. INTRODUCTION

Graphene is a material with point bandgap structure owing to its two-dimensional honeycomb crystal lattice, and it has many remarkable optoelectronic properties such as ultrawideband absorption [1], controllable interband transition [2], and nonlinear saturable absorption [3]. Recently, many graphene-based devices have been demonstrated including photodetectors [4], broadband polarizers [5], optical modulators [6,7], and ultrafast pulsed lasers [8,9]. These devices mainly employ the optical absorption characteristic of graphene. For the incident light normal to the monolayer graphene layer, the constant absorption coefficient is ~2.3%. Considering the 0.33 nm thickness of monolayer graphene, the absorption is remarkably high. In this case, however, the interaction length between the optical field and the graphene is limited to the thickness of graphene. In order to achieve longer light/graphene interaction length, the graphene can be integrated on the surface of the waveguide or attached on a special fiber, and the interaction length is adjustable. In such graphene/waveguide or fiber structures, the evanescent field of the propagating light interacts with the graphene covering on their surface. Such a technique has been implemented to realize the silicon-on-insulator waveguide-integrated double-layer graphene electroabsorption modulator [6], broadband graphene-based fiber polarizer [5], nonlinear modes in graphene dielectric waveguide [10], and graphene-based microfiber saturable absorber (SA) [11].

As a novel SA, graphene exhibits outstanding optical properties, such as ultrafast recovery time and ultrabroad operation bandwidth [1]. The graphene-based SA is superior to the semiconductor saturable absorber mirror (SESAM) and single-wall carbon nanotubes (SWCNTs) as it does not require bandgap design and diameter control to improve its performance [12], which leads to intensive investigation on it in the development of passively mode-locked fiber lasers [13–21]. In general, graphene or graphene composites are prepared by mechanical exfoliation of graphene from bulk graphite [22,23], self-assembled graphene membrane [24], graphene-polyvinyl alcohol composite [12,25], few-layered graphene oxide solution [26], graphene nanoparticles from bulk graphite [27], chemical vapor deposition (CVD) synthetic multilayer graphene on Ni film with SiO_2/Si substrate [28–30], and CVD synthetic monolayer graphene on polycrystalline Cu substrate [31,32].

To activate the interaction of the evanescent field of optical fiber with graphene, the SAs have been fabricated by covering the surface of the microfiber [11], tapered fiber [33], and side-polished D-shaped fiber [34] with graphene. When compared with microfiber and tapered fiber, the D-shaped fiber is slightly robust and can be easily and tightly attached with saturable absorption material. The SWCNTs-deposited D-shaped fiber for passively mode-locked fiber lasers has been reported [35,36]. More recently, the mode-locked fiber lasers based on graphene oxide-deposited D-shaped fiber SA had

been demonstrated for producing femtosecond pulses [37,38]. Owing to the asymmetric structure of the D-shaped fiber, the graphene-based SA has a high polarization-dependent loss (PDL), which leads to the polarization-sensitive saturable absorption.

The generation of solitons from passively mode-locked fiber lasers with net negative cavity dispersion is due to the natural balance between the cavity dispersion and the Kerr effect in optical fiber. Since both the gain and the loss exist, the solitons produced are essentially the dissipative solitons, whose dynamics is governed by the complex Ginzburg–Landau equation. The nonlinear coupling between the two polarization modes in the fiber laser results in vector solitons. The formation of vector solitons is influenced by the fiber birefringence, nonlinear Kerr effect, cavity gain, cavity loss, and cavity dispersion. A crucial condition for the vector soliton formation is that there are no polarization discrimination components used in the fiber laser cavity [28]. The strong polarization discrimination component could cause the nonlinear polarization rotation mode locking and would fix the polarization of light in the cavity to form scalar solitons. Adopting the polarization-insensitive graphene-based SA, the dissipative vector soliton operation [39], polarization rotation vector soliton operation [28], and the vector multisoliton operation [40] have been investigated experimentally. By the use of polarization-sensitive D-shaped fiber graphene oxide SA, the passively mode-locked fiber laser with different operation schemes, such as stable *Q*-switching, continuous-wave (CW) mode-locking and *Q*-switched mode-locking, have been investigated by simply tuning the polarization states in the laser cavity [37,38]. However, the soliton features of the lasers with polarization-sensitive SA are still unknown. In order to investigate the soliton features with strong polarization-sensitive SA, here we employ a few-layer graphene deposited D-shaped fiber SA with large PDL.

In this paper, the polarization-dependent SA of a few-layer graphene deposited D-shaped fiber is used to implement the passive mode-locking in an erbium-doped fiber (EDF) laser. The polarization-dependent absorption is measured experimentally and explained theoretically. It can be observed from experimental results that stable polarization-locked vector solitons could be obtained in the fiber lasers with high PDL, and the solitons are elliptically polarized solitons.

2. FABRICATION AND CHARACTERIZATION OF GRAPHENE-BASED SATURABLE ABSORBER

In order to obtain a large PDL, we use a D-shaped fiber covered with few-layer graphene. The side-polished D-shaped fiber is prepared by burnishing the single-mode fiber (SMF) with a grinding wheel, while using electrode discharge to improve its smoothness. The microscope image of the D-shaped fiber surface is shown in the upper part of Fig. 1(a), obtained by use of a Nikon Eclipse 80i microscope with 40× objective lens. The central cross section and the mode field are shown in the lower part of Fig. 1(a). The mode field is measured by use of a micronviewer (Model 7290A, Electrophysics) together with a microscope (IM7B, Atto Instruments). It can be clearly seen from Fig. 1(a) that the surface touches the fiber core, and the part of the mode field is exposed to air. The central region thickness of the D-shaped fiber is estimated

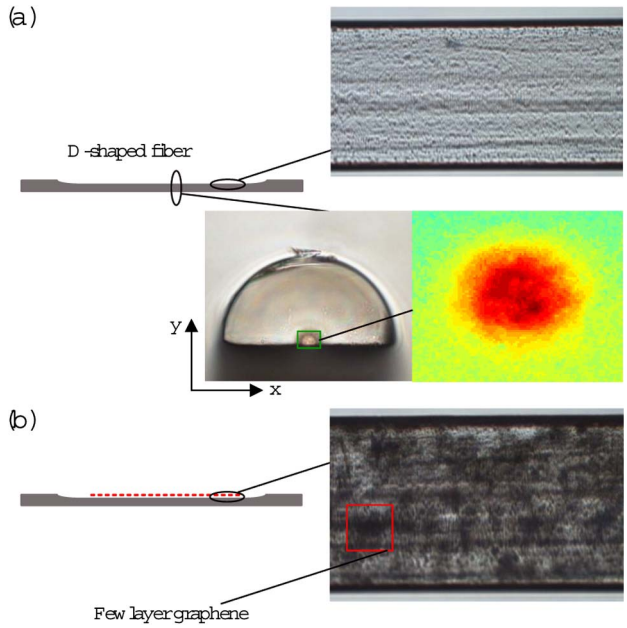

Fig. 1. (a) The upper photo is the surface of the D-shaped fiber, and the lower pictures are the cross section and mode field. (b) Microscope image of the surface with few-layer graphene.

to be ~64 μm from the cross section. The total length of the D-shaped fiber is ~2 cm, and the length of the central region is about 1 cm, which increases the interaction between the evanescent field and graphene. Its minimum insertion loss and PDL are measured to be ~13 and ~0.6 dB at the wavelength of 1550 nm, respectively. Figure 1(b) illustrates the surface of the D-shaped fiber covered with few-layer graphene. The few-layer graphene film is directly synthesized by use of the CVD method on Ni substrate (Graphene Supermarket). The graphene/Ni/Si layer is soaked with 0.05 mg/ml $FeCl_3$ solution to remove the Ni layer, and the large-area few-layer graphene film is then thoroughly transferred into the de-ionized water to soak and rinse several times. The length of the grephene is ~10 mm. After cleaning the polished surface of the D-shaped fiber with 99.5% propyl alcohol, the fiber is immersed slowly beneath the graphene/water interface. Followed by a gentle scooping of the graphene sheet onto the fiber, the SA is finished and the graphene can interact with the evanescent field.

The graphene or graphene oxide-deposited D-shaped fibers have nonnegligible PDL due to the asymmetry structure of the fiber [5,37], which can be measured by using a tunable CW light source in the telecommunication band (1500–1600 nm) together with a polarizer, and the experimental setup is schematically shown in Fig. 2(a). By adjusting the polarization controller (PC), the polarization direction of the incident light can be adjusted, and the output maximum corresponds to TE light [x-axis polarization in Fig. 1(a)] while the output minimum corresponds to TM light (y-axis polarization). With 0 dBm CW output power, the measured PDL values are shown in Fig. 2(b). It can be noticed that the PDL is irregular as a function of wavelength and has the values of ~20 dB and ~2.5 dB at 1550 and 1600 nm, respectively. The irregularity may originate from the mode field change with the wavelength as the D-shaped fiber is polished into the fiber core with a depth of ~2 μm. In order to verify the measured results, we analyze the PDL with a photonic all-parameter analyzer (81910A, Agilent), and the analyzed data are shown in Fig. 2(b). It is

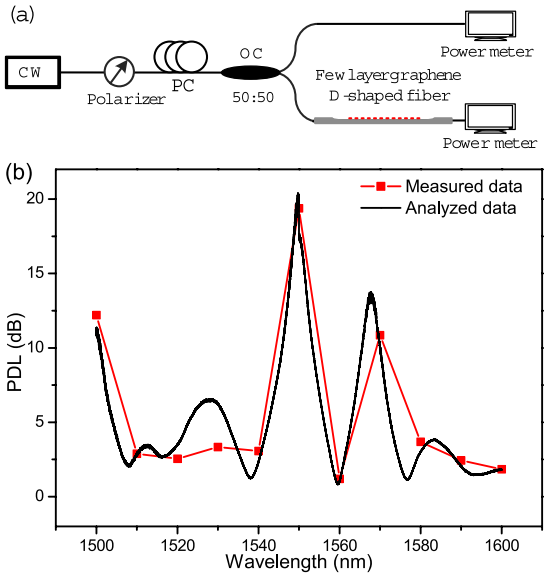

Fig. 2. (a) Measurement system for PDL of the graphene-based SA. (b) The measured PDL as a function of wavelength.

found that the results obtained in the measurement are consistent with those obtained from the parameter analyzer.

The PDL of the D-shaped fiber with graphene is much higher than that without graphene. For further insight, we consider the thin layer graphene is a perturbative absorption for the light field of the D-shaped fiber without graphene. For the unperturbed situation, according to waveguide theory the boundary conditions for the TE and TM modes are expressed by [41]

$$\hat{\mathbf{n}} \times (\mathbf{E}_2 - \mathbf{E}_1) = 0\,(\mathbf{TE}), \tag{1}$$

$$\hat{\mathbf{n}} \cdot (\mathbf{D}_2 - \mathbf{D}_1) = 0\,(\mathbf{TM}), \tag{2}$$

where $\hat{\mathbf{n}}$ is along the y-axis, $\mathbf{E}_2$, $\mathbf{D}_2$ are the fields on the air side of the interface, $\mathbf{E}_1$, $\mathbf{D}_1$ are the corresponding fields on the fiber side of the interface. So the electric field is continuous for the TE mode, and the electric displacement field is continuous for the TM mode. Since $\mathbf{D}_{1,2} = \varepsilon_{1,2}\mathbf{E}_{1,2}$ (where $\varepsilon_{1,2}$ are dielectric constants for fiber or air), the electric field on the air side of the interface for the TM mode is larger than that for the TE mode, thus the TM mode suffers higher absorption loss when the D-shaped fiber is covered with graphene.

Figure 3(a) schematically shows the experimental configuration for measurement of polarization-dependent absorption of the graphene-based SA. A femtosecond fiber laser (central wavelength 1552.19 nm, pulse width of ~2 ps, and repetition rate of 20 MHz, PriTel FFL-700) is amplified by an erbium-doped fiber amplifier (EDFA, Amonics). After passing through a polarizer, the polarized light controlled by an adjacent PC, is injected into graphene-based SA via an attenuator (ATT) and a 10:90 optical coupler (OC) [42]. Within the output power range of the pulsed fiber laser, the polarization-dependent absorption of graphene-based SA is measured and the results obtained are shown in Fig. 3(b). When the average output power is raised from 0.3 to 11 mW, the transmission increases by ~2% for the TE mode and ~1.3% for the TM mode.

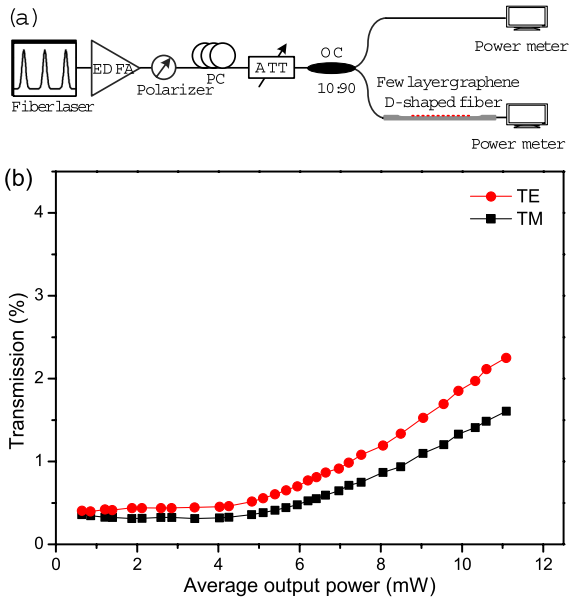

Fig. 3. (a) Schematic experimental setup for the measurement of polarization-dependent absorption of the graphene-based SA. (b) The measured nonlinear absorption of the graphene-based SA for TE mode and TM mode.

3. EXPERIMENTAL SETUP

The passively mode-locked EDF laser with a ring cavity configuration is presented in Fig. 4. A 1.6 m high concentration EDF (OFS EDF-80) is used as the gain medium, pumped by a 1480 nm high power laser diode (Anritsu AF4B150FA75L) through a 1480/1550 nm wavelength division multiplexer (WDM) coupler. An intracavity PC is used to optimize the mode-locking operation while a polarization-independent isolator maintains the unidirectional laser pulse propagation. The graphene-based SA is inserted in the cavity between the PC and OC. A section of SMF with 10 m in length is inserted into the cavity to adjust the total cavity dispersions. The PDLs of the OC, WDM, and optical isolator are less than 0.1 dB. The mode-locked pulses can be directed out by use of a 90:10 coupler connecting with another polarization-independent isolator. The group velocity dispersion (GVD) plays an important role in maintaining the mode-locked fiber laser stability. The GVD of the EDF used in the system is –46.25 ps/nm/km

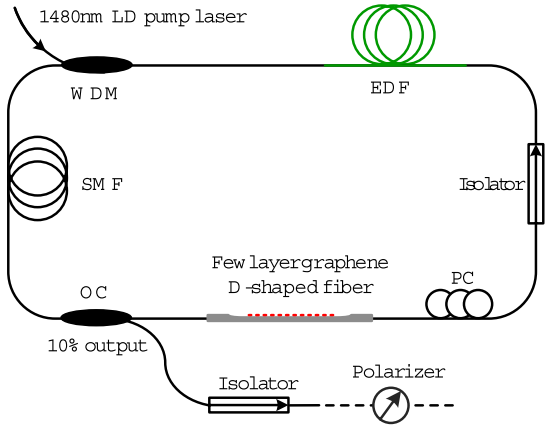

Fig. 4. Experimental setup of the few-layer graphene deposited D-shaped fiber mode-locked laser.

and that of the SMF is 18 ps/nm/km, at the wavelength of 1560 nm. The total laser cavity length is ~21 m, thus the round-trip dispersion of the whole cavity is $\sim -0.32\ \mathrm{ps}^2$, which ensures that the cavity has net anomalous GVD.

4. RESULTS AND DISCUSSION

First, the pump power is fixed at 230 mW, and the polarizer is not connected to the output port of the fiber laser. The laser optical spectrum is obtained by use of an optical spectrum analyzer (ANDO AQ6319) with 0.01 nm resolution. The fiber laser is easily tuned to operate in the CW state, and the corresponding optical spectrum is shown in Fig. 5(a). There are two peaks in the spectrum, the left one centered at ~1532 nm is the peak of the gain spectrum of the EDF. In CW operation the spontaneous gain is not completely suppressed because of the large loss of the graphene-based SA. By slightly tuning the PC, the fiber laser can operate in a stable mode-locking state, and its optical spectrum is also shown in Fig. 5(a), where it can be found that the spontaneous gain is further suppressed. The central wavelength is 1553 nm, and the FWHM bandwidth value is ~5 nm. The Kelly sidebands, resulting from the intracavity periodical perturbation, clearly appear with discrete and well-defined peaks in the optical spectrum. The pulse intensity profile is monitored by a second-harmonic generation autocorrelator (FEMTOCHROME FR-103XL, resolution <5 fs) and recorded by an oscilloscope (Tektronix, TPS 2024). Figure 5(b) demonstrates the recorded AC trace of the laser pulses, and the pulse width of 1.3 ps can be observed for a sech^2 curve fit. Considering its decorrelation factor of 0.648, the actual pulse width is ~842 fs. The time-bandwidth product of the pulses is 0.518, indicating that the soliton pulses are chirped. The chirp may originate from the net dispersion in the laser cavity [43].

The pulse train is measured by use of a high-speed photodetector (Newfocus 1414, 25 GHz), which is connected to the same oscilloscope. The pulse train of the laser output shown in Fig. 6(a) has a period of 107.9 ns, which matches well with the cavity round-trip time and verifies that the laser is mode locked. To study the operation stability, we have measured the radio frequency (RF) spectrum of the passively mode-locked fiber laser by the high-speed photodetector together with a real-time spectrum analyzer (Tektronix RSA 3303A, 3 GHz). The fundamental peak is located at the repetition rate of 9.248 MHz, as shown in Fig. 6(b), with a signal-to-noise ratio (SNR) of 70 dB. The inset of Fig. 6(b) shows the higher order of harmonic RF spectrum up to 200 MHz, in which the high SNR can also be observed, indicating the good mode-locking stability. The average output power is ~8.93 dBm, with pulse energy of ~0.845 nJ.

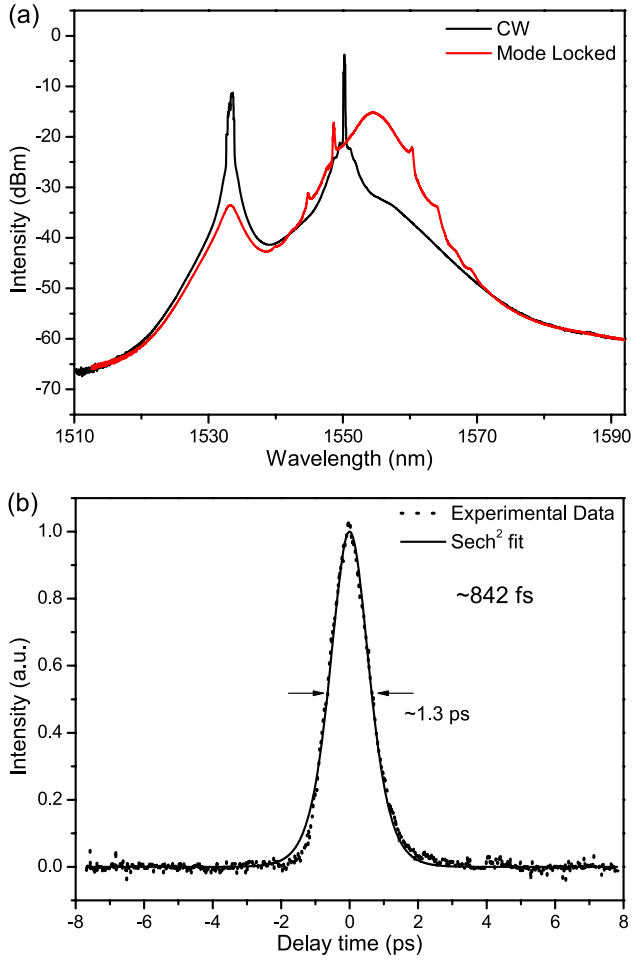

Fig. 5. (a) Output optical spectrums for CW and passively mode-locked fiber lasers. (b) Mode-locked pulse shape (experimental data) with Sech^2 fit.

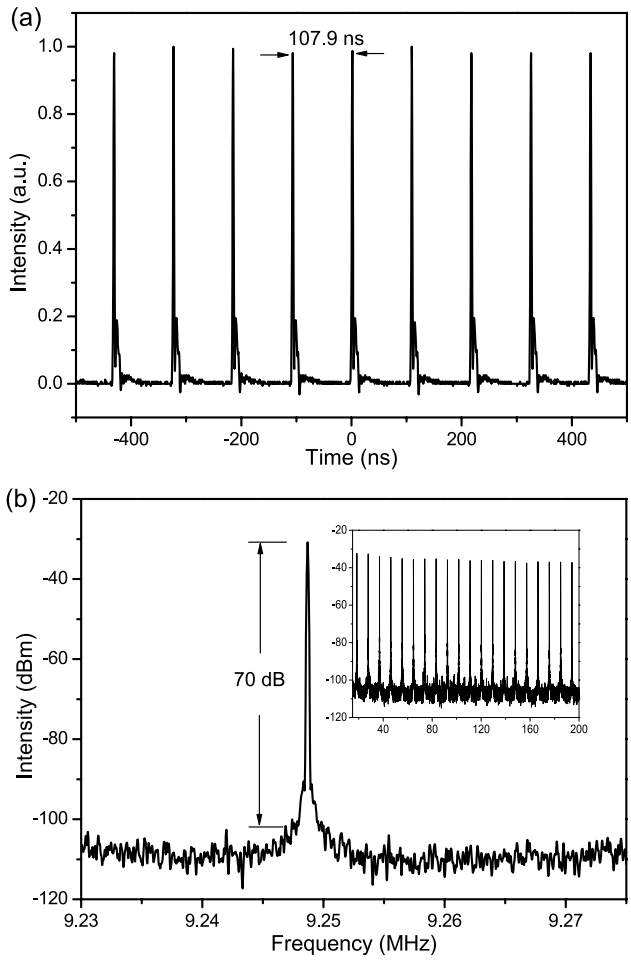

Fig. 6. (a) Typical laser output pulse trains. (b) RF spectrum measured around the fundamental repetition rate, and the inset is the RF spectrum with high-order harmonic of the repetition rate.

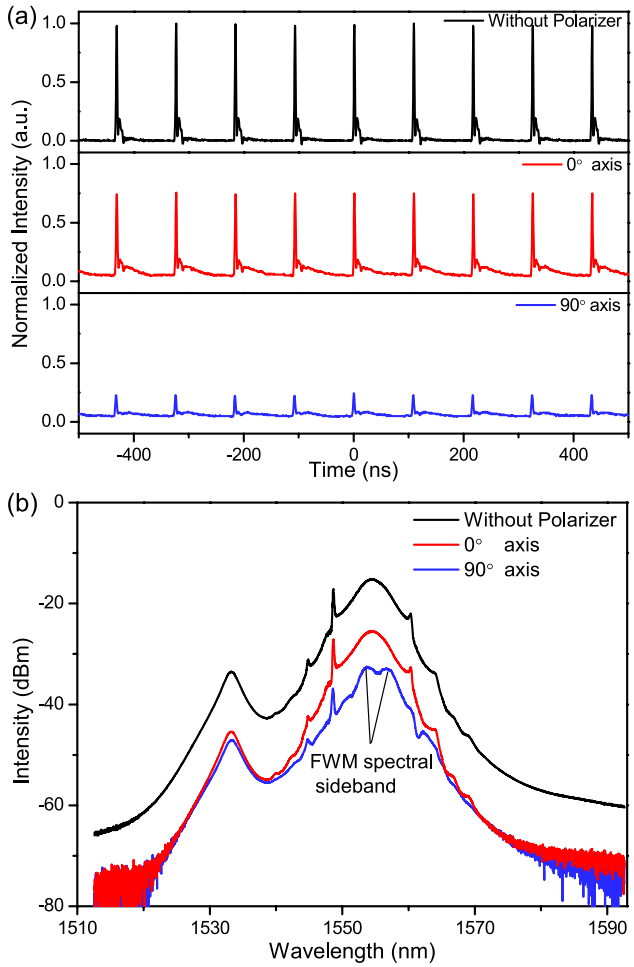

Fig. 7. (a) Pulse trains of the polarization-locked vector soliton. (b) Optical spectrums of the polarization-locked vector soliton.

To experimentally resolve the two orthogonal polarization components of the solitons, a polarizer is connected to the output port of the fiber laser, as shown in Fig. 4. By tuning the polarizer, the polarization angle is set at 0° when the output power is the maximum, thus the other orthogonal polarization direction is 90°. Figure 7 shows the state of the polarization-locked soliton operation of the laser. After the polarizer, the two orthogonal polarization pulse traces show uniform pulse trains, as demonstrated in Fig. 7(a). That is, all vector solitons in the cavity keep the same pulse intensity after each cavity trip. Furthermore, all vector solitons have exactly same polarization and the polarization features keep unchanged inside or outside of the cavity. In addition, it is found that the intensity for the 90° polarization becomes the minimum, much lower than the intensity of the 0° polarization, and the intensity ratio obtained is ~0.321. This indicates that the solitons are elliptical polarization due to the high PDL. Figure 7(b) shows the optical spectrums of the pulses along two orthogonal polarization directions and the total pulse without polarizer. The soliton spectrum along the 0° and 90° polarization directions have different spectral profiles and sidebands, indicating that the solitons are vector solitons.

The formation of vector solitons is determined by the combination of the nonlinear polarization evolution of two polarization components and the mode locking by a SA [44,45]. Based on the coupled complex Ginzburg–Landau equations for the two polarization components, the polarization-locked vector solitons have been theoretically studied, and elliptically polarized solitons may be generated for certain laser operation parameters [46]. With the high PDL graphene-based SA, the absorption for the TE mode is much lower than that of the TM mode. Therefore, the intracavity pulse energy of the TE mode is much higher than that of the TM mode for a fixed pump power. The coherence energy exchange occurs among the two orthogonal polarization components through the four-wave mixing (FWM) process [47], and the FWM spectral sidebands could form on the polarization resolved spectrum of the vector solitons, as shown in Fig. 7(b). Since the FWM process is the internal process of the vector soliton and the 0° polarization component intensity is high enough, no FWM spectral sidebands appear on the total and 0° polarization soliton spectrums. It is noted that the FWM sidebands are strong on the weak 90° polarization soliton spectrum. These experimental results suggest that the 90° polarization soliton may be created by FWM and cavity birefringence-induced cross-phase modulation [48]. In addition, no polarization rotation vector solitons are observed by slightly tuning the intracavity PC [49,50]; it proves that it is difficult to transfer energy from the 90° polarization soliton to the 0° polarization one, since the loss of the 90° polarization component is much larger than that of the 0° polarization component.

5. CONCLUSION

In conclusion, we have experimentally investigated the polarization-locked vector soliton operation of a mode-locked laser with a few-layer graphene deposited D-shaped fiber. It demonstrated that the resonant energy transfer between two orthogonal polarization components induces the elliptical polarization vector solitons with the large PDL of graphene-based SA. As the SA is highly polarization sensitive, our work may provide a new insight for the dynamics of vector solitons.

ACKNOWLEDGMENTS

The authors are pleased to acknowledge support from the Hong Kong Polytechnic University research grants 4-ZZE6 and G-YM19.

REFERENCES

1. F. Bonaccorso, Z. Sun, T. Hasan, and A. Ferrari, "Graphene photonics and optoelectronics," Nat. Photonics **4**, 611–622 (2010).
2. F. Wang, Y. Zhang, C. Tian, C. Girit, A. Zettl, M. Crommie, and Y. R. Shen, "Gate-variable optical transitions in graphene," Science **320**, 206–209 (2008).
3. Q. Bao, H. Zhang, Y. Wang, Z. Ni, Y. Yan, Z. X. Shen, K. P. Loh, and D. Y. Tang, "Atomic-layer graphene as a saturable absorber for ultrafast pulsed lasers," Adv. Funct. Mater. **19**, 3077–3083 (2009).
4. T. Mueller, F. Xia, and P. Avouris, "Graphene photodetectors for high-speed optical communications," Nat. Photonics **4**, 297–301 (2010).
5. Q. Bao, H. Zhang, B. Wang, Z. Ni, C. H. Y. X. Lim, Y. Wang, D. Y. Tang, and K. P. Loh, "Broadband graphene polarizer," Nat. Photonics **5**, 411–415 (2011).
6. M. Liu, X. Yin, and X. Zhang, "Double-layer graphene optical modulator," Nano Lett. **12**, 1482–1485 (2012).
7. C. Xu, Y. Jin, L. Yang, J. Yang, and X. Jiang, "Characteristics of electro-refractive modulating based on graphene-oxide-silicon waveguide," Opt. Express **20**, 22398–22405 (2012).
8. Z. Sun, T. Hasan, F. Torrisi, D. Popa, G. Privitera, F. Wang, F. Bonaccorso, D. M. Basko, and A. C. Ferrari, "Graphene mode-locked ultrafast laser," ACS Nano **4**, 803–810 (2010).

9. Z. Sun, D. Popa, T. Hasan, F. Torrisi, F. Wang, E. J. Kelleher, J. C. Travers, V. Nicolosi, and A. C. Ferrari, "A stable, wideband tunable, near transform-limited, graphene-mode-locked, ultrafast laser," Nano Res. **3**, 653–660 (2010).
10. A. Auditore, C. De Angelis, A. Locatelli, S. Boscolo, M. Midrio, M. Romagnoli, A. D. Capobianco, and G. Nalesso, "Graphene sustained nonlinear modes in dielectric waveguides," Opt. Lett. **38**, 631–633 (2013).
11. X. He, Z. B. Liu, D. N. Wang, M. Yang, C. Liao, and X. Zhao, "Passively mode-locked fiber laser based on reduced graphene oxide on microfiber for ultra-wide-band doublet pulse generation," J. Lightwave Technol. **30**, 984–989 (2012).
12. D. Popa, Z. Sun, F. Torrisi, T. Hasan, F. Wang, and A. Ferrari, "Sub 200 fs pulse generation from a graphene mode-locked fiber laser," Appl. Phys. Lett. **97**, 203106 (2010).
13. H. Zhang, Q. Bao, D. Tang, L. Zhao, and K. Loh, "Large energy soliton erbium-doped fiber laser with a graphene-polymer composite mode locker," Appl. Phys. Lett. **95**, 141103 (2009).
14. H. Zhang, D. Tang, R. Knize, L. Zhao, Q. Bao, and K. P. Loh, "Graphene mode locked, wavelength-tunable, dissipative soliton fiber laser," Appl. Phys. Lett. **96**, 111112 (2010).
15. H. Zhang, D. Tang, L. Zhao, Q. Bao, K. Loh, B. Lin, and S. Tjin, "Compact graphene mode-locked wavelength-tunable erbium-doped fiber lasers: from all anomalous dispersion to all normal dispersion," Laser Phys. Lett. **7**, 591–596 (2010).
16. J. Sotor, G. Sobon, K. Krzempek, and K. M. Abramski, "Fundamental and harmonic mode-locking in erbium-doped fiber laser based on graphene saturable absorber," Opt. Commun. **285**, 3174–3178 (2012).
17. P. L. Huang, S. C. Lin, C. Y. Yeh, H. H. Kuo, S. H. Huang, G. R. Lin, L. J. Li, C. Y. Su, and W. H. Cheng, "Stable mode-locked fiber laser based on CVD fabricated graphene saturable absorber," Opt. Express **20**, 2460–2465 (2012).
18. J. Xu, S. Wu, J. Liu, Q. Wang, Q. H. Yang, and P. Wang, "Nanosecond-pulsed erbium-doped fiber lasers with graphene saturable absorber," Opt. Commun. **285**, 4466–4469 (2012).
19. W. Cao, H. Wang, A. Luo, Z. Luo, and W. Xu, "Graphene-based, 50 nm wide-band tunable passively *Q*-switched fiber laser," Laser Phys. Lett. **9**, 54–58 (2012).
20. B. Fu, L. Gui, W. Zhang, X. Xiao, H. Zhu, and C. Yang, "Passive harmonic mode locking in erbium-doped fiber laser with graphene saturable absorber," Opt. Commun. **286**, 304–308 (2013).
21. Q. Sheng, M. Feng, W. Xin, T. Han, Y. Liu, Z. Liu, and J. Tian, "Actively manipulation of operation states in passively pulsed fiber lasers by using graphene saturable absorber on microfiber," Opt. Express **21**, 14859–14866 (2013).
22. Y. M. Chang, H. Kim, J. H. Lee, and Y. W. Song, "Multilayered graphene efficiently formed by mechanical exfoliation for nonlinear saturable absorbers in fiber mode-locked lasers," Appl. Phys. Lett. **97**, 211102 (2010).
23. J. Sotor, G. Sobon, and K. M. Abramski, "Scalar soliton generation in all-polarization-maintaining, graphene mode-locked fiber laser," Opt. Lett. **37**, 2166–2168 (2012).
24. L. Gui, W. Zhang, X. Li, X. Xiao, H. Zhu, K. Wang, D. Wu, and C. Yang, "Self-assembled graphene membrane as an ultrafast mode-locker in an erbium fiber laser," IEEE Photon. Technol. Lett. **23**, 1790–1792 (2011).
25. S. Y. Choi, D. K. Cho, Y. W. Song, K. Oh, K. Kim, F. Rotermund, and D. I. Yeom, "Graphene-filled hollow optical fiber saturable absorber for efficient soliton fiber laser mode-locking," Opt. Express **20**, 5652–5657 (2012).
26. Z. B. Liu, X. He, and D. N. Wang, "Passively mode-locked fiber laser based on a hollow-core photonic crystal fiber filled with few-layered graphene oxide solution," Opt. Lett. **36**, 3024–3026 (2011).
27. Y. H. Lin, C. Y. Yang, J. H. Liou, C. P. Yu, and G. R. Lin, "Using graphene nano-particle embedded in photonic crystal fiber for evanescent wave mode-locking of fiber laser," Opt. Express **21**, 16763–16776 (2013).
28. Y. F. Song, H. Zhang, D. Y. Tang, and D. Y. Shen, "Polarization rotation vector solitons in a graphene mode-locked fiber laser," Opt. Express **20**, 27283–27289 (2012).
29. G. Sobon, J. Sotor, and K. M. Abramski, "Passive harmonic mode-locking in Er-doped fiber laser based on graphene saturable absorber with repetition rates scalable to 2.22 GHz," Appl. Phys. Lett. **100**, 161109 (2012).
30. J. Du, S. Zhang, H. Li, Y. Meng, X. Li, and Y. Hao, "L-band passively harmonic mode-locked fiber laser based on a graphene saturable absorber," Laser Phys. Lett. **9**, 896 (2012).
31. Q. Bao, H. Zhang, Z. Ni, Y. Wang, L. Polavarapu, Z. Shen, Q. H. Xu, D. Tang, and K. P. Loh, "Monolayer graphene as a saturable absorber in a mode-locked laser," Nano Res. **4**, 297–307 (2011).
32. X. He, Z. Liu, and D. N. Wang, "Wavelength-tunable, passively mode-locked fiber laser based on graphene and chirped fiber Bragg grating," Opt. Lett. **37**, 2394–2396 (2012).
33. J. Wang, Z. Luo, M. Zhou, C. Ye, H. Fu, Z. Cai, H. Cheng, H. Xu, and W. Qi, "Evanescent-light deposition of graphene onto tapered fibers for passive *Q*-switch and mode-locker," IEEE Photon. J. **4**, 1295–1305 (2012).
34. Y. W. Song, S. Y. Jang, W. S. Han, and M. K. Bae, "Graphene mode-lockers for fiber lasers functioned with evanescent field interaction," Appl. Phys. Lett. **96**, 051122 (2010).
35. Y. W. Song, S. Yamashita, C. S. Goh, and S. Y. Set, "Carbon nanotube mode lockers with enhanced nonlinearity via evanescent field interaction in D-shaped fibers," Opt. Lett. **32**, 148–150 (2007).
36. S. Wang, Y. Pan, R. Gao, X. Zhu, X. Su, and S. Qu, "Mode-locked double-clad fiber laser with a carbon nanotubes saturable absorber," Acta Phys. Sin. **62**, 024209 (2013).
37. M. Jung, J. Koo, J. Park, Y. W. Song, Y. M. Jhon, K. Lee, S. Lee, and J. H. Lee, "Mode-locked pulse generation from an all-fiberized, Tm-Ho-codoped fiber laser incorporating a graphene oxide-deposited side-polished fiber," Opt. Express **21**, 20062–20072 (2013).
38. J. Lee, J. Koo, P. Debnath, Y. Song, and J. Lee, "A *Q*-switched, mode-locked fiber laser using a graphene oxide-based polarization sensitive saturable absorber," Laser Phys. Lett. **10**, 035103 (2013).
39. H. Zhang, D. Tang, L. Zhao, Q. Bao, and K. P. Loh, "Vector dissipative solitons in graphene mode locked fiber lasers," Opt. Commun. **283**, 3334–3338 (2010).
40. Y. F. Song, L. Li, H. Zhang, D. Y. Shen, D. Y. Tang, and K. P. Loh, "Vector multi-soliton operation and interaction in a graphene mode-locked fiber laser," Opt. Express **21**, 10010–10018 (2013).
41. G. W. Hanson, "Quasi-transverse electromagnetic modes supported by a graphene parallel-plate waveguide," J. Appl. Phys. **104**, 084314 (2008).
42. T. Hasan, Z. Sun, F. Wang, F. Bonaccorso, P. H. Tan, A. G. Rozhin, and A. C. Ferrari, "Nanotube–polymer composites for ultrafast photonics," Adv. Mater. **21**, 3874–3899 (2009).
43. K. Kashiwagi and S. Yamashita, "Deposition of carbon nanotubes around microfiber via evanescent light," Opt. Express **17**, 18364–18370 (2009).
44. S. Smirnov, S. Kobtsev, S. Kukarin, and S. Turitsyn, "Mode-locked fibre lasers with high-energy pulses," in *Laser Systems for Applications* (InTech, 2011).
45. W. H. Renninger and F. W. Wise, "Dissipative soliton fiber lasers," in *Fiber Lasers* (Wiley, 2012), pp. 97–133.
46. J. Soto-Crespo, N. Akhmediev, B. Collings, S. Cundiff, K. Bergman, and W. Knox, "Polarization-locked temporal vector solitons in a fiber laser: theory," J. Opt. Soc. Am. B **17**, 366–372 (2000).
47. H. Zhang, D. Tang, L. Zhao, and N. Xiang, "Coherent energy exchange between components of a vector soliton in fiber lasers," Opt. Express **16**, 12618–12623 (2008).
48. H. Zhang, D. Tang, L. Zhao, and H. Tam, "Induced solitons formed by cross-polarization coupling in a birefringent cavity fiber laser," Opt. Lett. **33**, 2317–2319 (2008).
49. L. Zhao, D. Tang, H. Zhang, and X. Wu, "Polarization rotation locking of vector solitons in a fiber ring laser," Opt. Express **16**, 10053–10058 (2008).
50. L. Zhao, D. Tang, X. Wu, H. Zhang, and H. Tam, "Coexistence of polarization-locked and polarization-rotating vector solitons in a fiber laser with SESAM," Opt. Lett. **34**, 3059–3061 (2009).